Microfabrication Using Elastomeric Stamp Deformation

Xiaojuan Fan, Dat T. Tran, Daniel P. Brennan, and Scott R. J. Oliver*

Department of Chemistry and Biochemistry, University of California, 1156 High Street, Santa Cruz, California 95064

Received: August 11, 2005; In Final Form: March 24, 2006

Elastomeric stamp deformation has been utilized for the contact printing (CP) of self-assembled monolayers (SAMs) and, more recently, polymers and proteins. Here, we take advantage of this well-studied phenomenon to fabricate a series of new metal thin-film patterns not present on the original stamp. The rounded patterns are of nanoscale thickness, long-range order, and are created from elastomeric stamps with only straight-edged features. The metal was printed onto the surface of an α,ω-alkanedithiol self-assembled monolayer (SAM). The new shapes are controlled by a combination of stamp geometry design and the application of external pressure. Previously published rules on stamp deformation for contact printing of SAMs are invalid because the coating is instead a thin-metal film. This method represents a new pathway to micropatterning metal thin films, leading to shapes with higher complexity than the original lithographic masters.

Introduction

Metal thin-film patterns with complex shapes are used extensively in microelectronics for magnetic data storage,[1] photonic band gap crystals,[2,3] optical waveguides,[4] LEDs,[5] and biosensors.[6] There are many mature technologies for patterning metal thin films, such as optical lithography,[7−9] e-beam writing,[10,11] focused ion beam (FIB) writing,[12] and dip-pen nanolithography.[13] Several of these techniques are capable of creating complex nanometer scale features, but their inherent high cost renders them inaccessible for many researchers.

Contact printing (CP) of SAMs, pioneered by Whitesides and co-workers,[14,15] is a rapid, easy, and inexpensive alternative to thin-film formation. The benefits of this method include pattern delivery under ambient conditions and no need for post-etching steps. The elastomeric stamp can be fabricated by casting and curing an elastomer [poly(dimethylsiloxane), PDMS], against a photoresist master with the inverse of the desired patterns. Peeling off the stamp from the master is straightforward due to the poor adhesion between the two surfaces. CP has been used to create complex biological patterns using multileveled PDMS stamps, where pressure applied to the back partially compressed the stamp such that protein on the recessed regions came into contact with the substrate.[16] CP with stamp deformation can similarly be used for patterning polymer films. A ring-like polymer pattern was made by contacting a flat PDMS pad coated with poly(methyl methacrylate) (PMMA) on a patterned substrate with relatively deep trenches.[17]

Rogers and co-workers recently extended CP from organic species, proteins, and polymers to metal thin films for the fabrication of organic-based transistors.[18−23] They evaporated a thin layer of Au onto a PDMS stamp and then laminated the gold by CP onto the surface of a 1,8-octanedithiol SAM, predeposited on a substrate such as GaAs.[21] The resultant Au/SAM/GaAs junctions show electrical transport through the molecular layer, whereas Au/GaAs shorting was observed when Au was thermally evaporated directly onto the 1,8-octanedithiol SAM on GaAs.[22] The metal CP patterns can be high resolution both laterally (<100 nm)[15,16−21] and vertically (<2 nm).[24] In all cases, the patterns simply replicate the raised stamp surface relief.

Deformation of the stamp can occur upon contact with the substrate due to the flexibility of the elastomer. The process has been well studied because it was always considered a problem for CP of SAMs. Delamarche et al. proposed a critical stamp parameter, height aspect ratio [$r = h/a$, height (h) divided by feature size (a)].[25] It was suggested that a stamp is susceptible to collapse during CP if its height aspect ratio r is less than 0.2. On the other hand, lateral instabilities occur if r is larger than 2, where the tall features bend and contact each other. No collapse is expected for r between 0.2 and 2.[25] Very recently, Sharp et al. defined three modes of stamp failure, namely buckling, lateral collapse, and roof collapse.[26] Roof collapse refers to contact of the basal plane of the stamp with the substrate, thus causing undesired printing between the raised portions of the stamp. Bietsch and Michel described another critical condition for the spreading of printed SAM patterns, "fill factor" [$f = (a/s)^2$, where a is the size of the feature and s is the center-to-center distance].[27] It was found that collapse occurred for $f \geq 6.25\%$, whereas no collapse was observed for larger fill factors.

In addition to stamp geometry, applied pressure is another important factor in stamp deformation. Hui et al. theoretically studied the dependence of printed SAM patterns on applied pressure.[28] They assumed the elastomer to be homogeneous and isotropic, with Young's modulus (E) between 0.1 and 10 MPa and Poisson's ratio of approximately 0.5. When roof collapse occurs, the maximum vertical displacement of the stamp (V_{max}, i.e., the feature height) can be expressed as:

$$V_{max} \approx \frac{6\sigma s}{4\pi E}\cosh^{-1}\left[\sec\left[\frac{(s-a)\pi}{2s}\right]\right] \qquad (1)$$

where σ is the minimal applied force necessary for deformation.

These studies were all motivated toward *avoiding* stamp deformation and employed SAM-coated elastomeric stamps.

* To whom correspondence should be addressed. E-mail: soliver@chemistry.ucsc.edu; Fax: 831-459-2935.

10.1021/jp054519z CCC: $33.50
Published on Web 05/25/2006

Stamp deformation, however, can generate new shapes by *not* replicating the stamp features and applied to other types of coating, such as nanoparticle thin films. Yang and co-workers coated a PDMS stamp having elevated round platforms with nanoparticles by the Langmuir−Blodgett technique.[29] Adding pressure to deform the stamp during CP gave rings and "antirings" of nanoparticles around the platforms. Their studies also simply replicated the shapes from the original round stamps and were based on oxide nanoparticles.

Here, we extend this strategy for the first time to metal thin-film patterns. We take advantage of the knowledge of stamp deformation to deliver a range of more complex features over the entire wafer surface, where the stamp requires only simple straight-edged features. Because the metal films are more rigid and thicker compared to an alkanethiol SAM precursor, the above deformation rules are rendered invalid. Multiple CP steps from the same stamp leads to further examples of shapes that can be created. We discuss the pattern dependence on stamp feature size, separation, height, and the application of pressure.

Experimental Section

The fabrication process begins with a Si wafer substrate (Ultrasil Corporation, 3" diameter, single side polished) on which Ti (5 nm adhesion layer) was e-beam evaporated, followed by Ag (100 nm). The latter acts as the bottom metal of the final metal−SAM−metal sandwich junction. In the vacuum chamber, the substrate was ∼30 cm away from the source, with an evaporation rate of 1.0 Å/s. Following literature methods, an α,ω-alkanedithiol SAM was then grown on the metal surface by submersing overnight in a 10 mM methyl ethyl ketone (MEK) solution of 1,10-decanedithiol [$HS(CH_2)_{10}SH$, TCI Chemical]. The substrate was then rinsed with MEK to remove physisorbed molecules and dried in a stream of N_2 gas.

A photolithographic mask with transparent squares or rectangles ranging in size from 50 μm to 2 mm was first designed using the software package L-Edit (for PC, Tanner Research Inc.) and then transferred to a GCA/Mann 3600F Pattern Generator at the Cornell Nanofabrication Facility (CNF) cleanroom. A commercial 5" glass plate coated with Cr and photoresist (S1813 positive type, Shipley Co.) was used as the pre-mask blank. An array of ∼5000 squares or rectangles was flashed by the Pattern Generator over ca. 1 h. The photoresist was then developed (AZ 300 MIF, Hoechst Celanese Co.), exposed Cr was etched (CR-14, Cyantec Co.), and the remaining photoresist was stripped (1165 Remover, Shipley Co.).

To create elastomeric stamps with the desired surface features, an inverse mold of photoresist was then fabricated in the cleanroom. The photoresist (Shipley 1405, positive type) was evenly dispersed on a Si wafer by spin coating (7 μm thick) and then baked at 90 °C for 120 s. The photoresist film was exposed to UV light for 8 s through the mask and then developed (AZ 300MIF, Hoechst Celanese Co.), rinsed with deionized water, and finally dried under an N_2 stream. A PDMS (Sylgard 184, Dow Chemical Co., 10:1 mass ratio of silicone elastomer to curing agent) positive stamp was then cast against the photoresist negative master. After degassing the PDMS prepolymer under vacuum and curing at 70 °C overnight, the stamp can be easily peeled away from the master.

An optically smooth and uniform layer of metal (20 nm thickness) was coated on the stamp surface by e-beam evaporation under the same operating conditions as above. The coated stamp was then placed metal side down on the 1,10-decanedithiol SAM surface. The weight of the stamp gave sufficient contact for CP to occur, and the metal spontaneously transferred from the stamp to the SAM-coated substrate. When manual pressure was applied during CP, it is considered to be larger than the minimal force according to eq 1. We assume a Young's modulus of 0.75 MPa, which is typical for PDMS with a 10:1 prepolymer to curing agent ratio.[25,28,29] Peeling away the PDMS stamp completes the pattern fabrication procedure. In all cases, the stamp returns to its original shape after deformation, allowing multiple steps of CP for the deposition of metal remaining on recessed areas of the stamp.

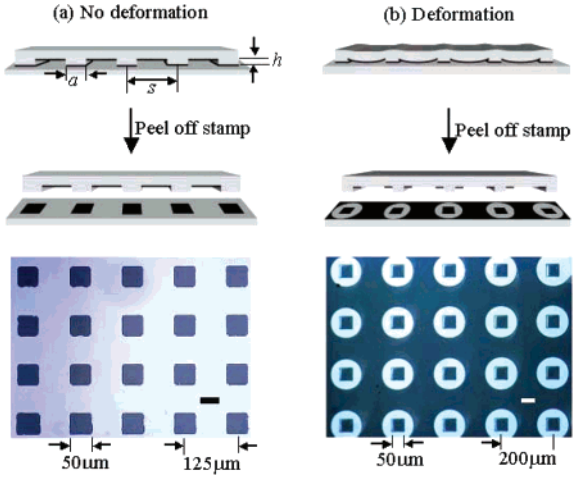

Figure 1. Schematic illustration of CP with or without stamp deformation, and corresponding optical micrographs of the resultant patterns [*a*: feature size; *s*: separation (center-to-center distance); *h*: feature height; scale bars: 50 μm]. (a) CP simply leads to squares that replicate the stamp features. (b) CP generates circular inverse patterns due to spontaneous stamp deformation.

Optical microscopy was performed on an Axioskop-2-MAT Microscope equipped with a CCD camera (Allied High Tech Products, Inc). Scanning electron microscope (SEM) photographs were obtained using an SEM (WB-6, International Scientific Instruments).

Results and Discussion

We have successfully fabricated Ag/SAM/Ag, Au/SAM/Au, and Au/Co/SAM/Co/Au patterned junction arrays through this approach. For simplicity, we selected Ag/SAM/Ag patterns as an initial example of the method. Figure 1 illustrates two different patterns created from almost identical stamps (Table 1, samples 1 and 2), an array of $50 \times 50 \times 7$ μm^3 raised squares but with different separations (Figure 1a: $s = 125$ μm; Figure 1b: $s = 200$ μm). Simple CP with no additional pressure resulted in distinct patterns, despite the stamps being almost identical. The stamp in Figure 1a created only metal squares on the SAM surface (dark areas), replicating the stamp shape. The stamp in Figure 1b transferred metal from not only the raised squares but also the stamp roof areas. Inverse circles thereby form around every metal square, with a diameter of ca. 125 μm, ∼2.5 times larger than the original square size ($a =$ 50 μm). The inverse circles (light color, Figure 1b) are areas where no contact occurred between the stamp and SAM surfaces due to the finite height ($h = 7$ μm) of the squares. Ca. 75% of the metal on the recessed roof area was transferred.

To account for these observations, several factors need to be considered, including stamp geometry, Young's modulus, and the application of external pressure. We will first focus on stamp geometry. All our samples have an aspect ratio of $r \leq 0.14$ (Table 1), which would predict collapse according to Delamarche ($r = h/a < 0.2$).[25] The lack of collapse in sample 1 (Figure

TABLE 1: Stamp Geometry, Height Aspect Ratio, and Fill Factor Values[a]

sample no.	shape	h (μm)	a (μm)	s (μm)	$r = h/a$, aspect ratio	$f = (a/s)^2$, fill factor (%)
1	square	7	50	125	0.14	16
2	square	7	50	200	0.14	6.25
3	rectangular	7	100 245	435 500	0.07 0.03	5.2 24
4	rectangular	7	100 300	280 385	0.07 0.02	12 61
5	square	7	50	150	0.14	11
6	rectangular	7	50 125	150 200	0.14 0.06	11 39
7	square	2	50	120	0.04	17
8	rectangular	2	50 300	250 600	0.04 0.007	4 25

[a] Two values, x and y, included for rectangular features.

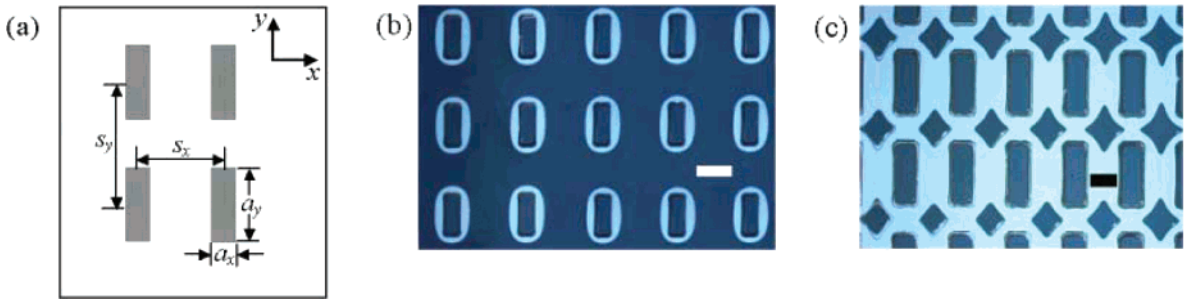

Figure 2. Micropatterns created from PDMS stamps with raised rectangular platforms. (a) Schematic of edge lengths (a_x, a_y) and center-to-center distances (s_x, s_y) along the x and y directions. (b) Sample 3 ($f_x = 5.2\%$ and $f_y = 24\%$) gives inverse oval shapes with rectangles in the centers (scale bar: 200 μm). (c) Sample 4 ($f_x = 12\%$ and $f_y = 61\%$) disfavors spontaneous deformation due to the larger f values, requiring external pressure to yield concave "diamonds" between the rectangles (scale bar: 100 μm).

1a) does agree with the fill factor rule of Sharpe et al. [$f = (a/s)^2 < 6.25\%$][26] due to the large fill factor f value of ~16%. Sample 2 in Figure 1b with $f = 6.25\%$ shows spontaneous roof collapse. Although the fill factor rule appears to override the height aspect ratio rule in predicting stamp collapse (the latter will not be considered further in the rest of this paper), both apply to stamps coated by SAMs. The lack of collapse here may be due to the rigidity of the metal film on the stamp surface tension, rendering the above rules inapplicable. Nonetheless, roof collapse allows the fabrication of metal micropatterns not present on the original stamp.

In the same manner, for sample 3, a PDMS stamp with rectangular raised features (schematic, Figure 2a: dimensions a_x, a_y, separation s_x, s_y along x and y, respectively) gave rise to an array of inverse oval shapes upon CP without external pressure (Figure 2b). The array has long-range order and is analogous to the inverse circles of Figure 1b. Spontaneous deformation occurred despite the high fill factor value along y of $f_y = 24\%$ (expected along x: $f_x = 5.2\%$). For rectangular stamps, collapse occurs even if only one direction follows the fill factor rule of $f \leq 6.25\%$.

The application of manual pressure during CP is equally important to stamp geometry in determining the pattern that is obtained. For experiments where manual pressure was applied, we assume it to be uniform, normal to the stamp, and greater than the minimum stress required for maximum vertical displacement (~0.14 MPa, deduced from eq 1 using a Young's modulus of 0.75 MPa as mentioned above). We designed a stamp with similar features but smaller separation (sample 4), such that $f_x = 12\%$ and $f_y = 61\%$, both much greater than 6.25%. If no external force is applied on the stamp, rectangular shapes are the only pattern, as expected (micrograph not shown). An external force renders the fill factor rule invalid. The printed Ag/SAM/Ag sandwich pattern becomes concave "diamonds" in the regions between four neighboring rectangles (Figure 2c). These patterns can also be considered as overlapped inverse ovals, following the outline around each rectangle. They are yet another example of new features not on the original stamp,

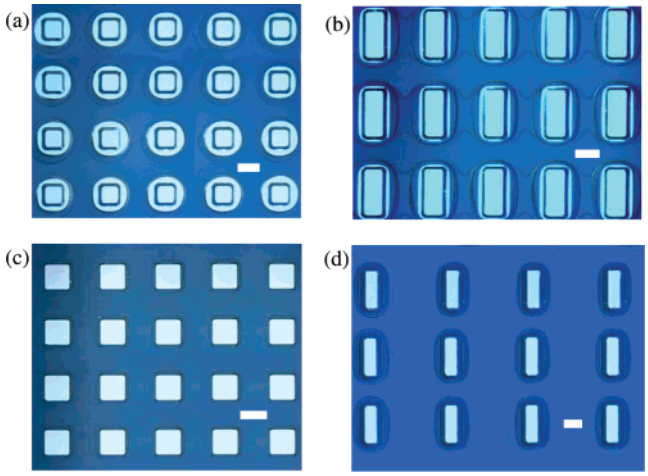

Figure 3. Two-step CP with manual pressure results in inverse circular (a) and oval (b) arrays, but with interior rims. Shorter stamp features eliminate the inner rings but also lead to only slightly rounded inverse square (c) and rectangular (d) arrays. Scale bars: 50 μm.

where the shape of the ovals is controlled through feature dimension and external pressure.

Because all patterns mentioned above have the original squares (or rectangles) inside the inverse circles (or ovals), we attempted to isolate the latter by a two-step CP process. Similar stamps with raised features ($h = 7$ μm) were used [squares: sample 5; rectangles: sample 6], and the resultant patterns are shown in Figure 3. In the first step, the stamp was brought into contact with a SAM surface in the absence of manual pressure. As expected for such high f values, only metal on the raised area of the stamp was transferred (micrograph not shown, but identical to Figure 1a). After the first contact, peeling away the stamp did not damage the metal remaining on the recessed area of the stamp. A second CP with manual pressure on a new α,ω-alkanedithiol SAM-coated substrate isolated the inverse circular (Figure 3a) and oval (Figure 3b) arrays. The external pressure therefore caused both stamps to deform despite the high fill

factors of 11 and 39% (>6.25%). Again we see that the fill factor rule is only valid in the absence of additional pressure.

The diameter of these inverse circles is about 100 μm, ~2 times larger than the square feature size (Figure 3a), whereas the ratio above was ~2.5 (low f value, no pressure, Figure 1b). The external force, not surprisingly, resulted in more roof area contacting the substrate. The inverse shapes generated by external pressure (Figure 3a,b) are also not as well-defined as those generated by spontaneous collapse (Figures 1b and 2b). The rims inside the shapes (Figure 3a,b) are likely due to residual metal on the raised portions after the first CP step. A stamp with receding sidewalls may eliminate these rims while retaining the inverse circular/oval features.

A shorter stamp might also be able to eliminate these rims due to shorter sidewalls. We fabricated a stamp with $h = 2$ μm (Table 1, sample 7) and repeated the two-step CP. During the second CP with pressure, the rims were not produced, but at the same time the stamp had less area of noncontact because of the shorter height (Figure 3c). As a result, an inverse square array was obtained, with only slightly rounded corners. These results indicate that stamp height is another key parameter in controlling the pattern that is obtained.

Similarly, we designed a stamp with shorter rectangles (Table 1, sample 8). Because $f_x = 4\% < 6.25\%$, collapse is expected during CP even though f_y is ~25%, as concluded above for Figure 2b. To deter elastomer deformation and prevent roof collapse during the first CP, we adhered a supporting plate (e.g., a glass slide or Si wafer) to the back of the stamp. Rectangle patterns were only transferred as expected (micrograph not shown), leaving metal on the recessed areas of the stamp. The supporting plate was then peeled away from the stamp. A second CP to a new SAM surface without pressure led to the inverse rectangles that were only slightly rounded at the corners (Figure 3d). The disappearance of inverse circles (Figure 3c) and ovals (Figure 3d) is attributed to the lower feature height (2 versus 7 μm, Table 1). Shorter features lead to greater roof contact with the substrate during the second CP. The reduced area of noncontact gives shapes that are closer to those of the original stamp.

Many other shapes should also be possible by this method, and we offer one example in Figure 4. A stamp with rows of offset squares and $r = 0.14$ (the value that gave inverse circles, Figure 1b) should lead to concave triangles via stamp deformation. The original square features would be hexagonally packed (Figure 4a), with a separation ~2.5 times larger than the edge size a, thus $f \approx 16\%$. This value is the same as the stamp in Figure 1a, but because of the offset layout, the expected pattern is triangles between the squares (Figure 4b). As for the concave diamond pattern of Figure 2c, external pressure would be necessary because of the high f value. The diameter of the circles is estimated to be $2.5a$ if the external force is uniform.

To eliminate the squares, a two-step CP process could be used. The first step would remove the metal on the raised squares only, where the stamp should not deform due to the large f value, as performed for sample 5 and 6. Releasing the stamp and a second CP with pressure on a new SAM substrate would isolate the triangular array (Figure 4c) with smaller feature size compared with the original squares. This process could lead to metal patterns *with higher resolution than that of the original stamp*. Microscale stamp relief could therefore lead to arrays of nanoscale patterns. Such 2D structure may be useful as a vertical waveguide for an optical laser "crystal" device if the pattern is created on a transparent substrate such as indium tin oxide.[3] The circle size and separation could be easily controlled by stamp design, for precise tuning of diffraction wavelength.

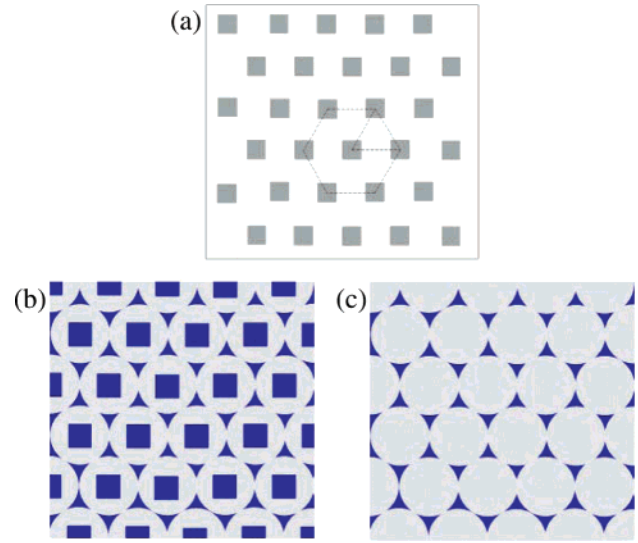

Figure 4. One example of shape design that is possible utilizing stamp deformation. (a) Original stamp with offset rows of squares (dark gray: raised square features on the stamp before coating with metal). (b) After coating the stamp with metal and performing CP, stamp deformation would generate an array of squares centered in inverse circles (blue: metal contact printed on the SAM surface). (c) A two-step CP process would eliminate the squares, isolating the array of concave triangles.

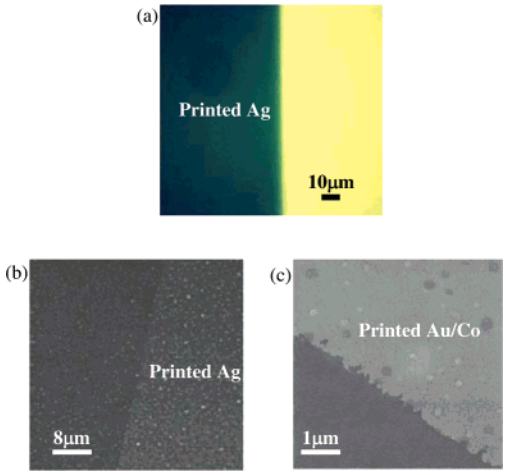

Figure 5. Micrographs of the edges of printed Ag films: (a) Optical micrograph (dark color is the substrate−Ag−SAM−Ag area); (b), (c) SEM images of contact printed Ag and Au/Co films, respectively.

Figure 5 is a series of images of the printed metals through the above approach. Figure 5a is an optical micrograph of the edge of a printed Ag film, showing a continuous coating. The corresponding SEM (Figure 5b) displays grains on the surface, for both the stamped (substrate−Ag−SAM−Ag) and unstamped (original substrate−Ag−SAM) areas. The overall grain size of the stamped area is smaller (Figure 5b), likely due to the fact that the printed top Ag film is thinner (20 nm) than the bottom Ag layer (100 nm). The mean edge roughness is estimated to be 0.5 μm. We also present the SEM of a stamped Au/Co layer (Figure 5c), with an average edge roughness of less than 0.25 μm. It was reported that edge roughness of a printed Au film can be as low as ca. 15 nm using a rigid stamp and a PDMS substrate.[19] Edge roughness of contact printed metal is typically determined by grain size, edge structure of the stamp, and the

efficiency of contact printing. The greater roughness for our samples is possibly due to larger grain size of metal Ag and Co on the original stamp. It may be possible to minimize surface edge roughness by optimizing evaporation conditions to obtain a smoother metal film on PDMS before stamping.

This approach of micropatterning a metal film on an organic terminated surface provides a promising alternative to conventional lithography for creating complex 2D features of ultrathin metal film. Metals easily transfer from the polymer stamp to molecular surface due to: (i) poor adhesion between PDMS and metal, likely due to the hydrophobic $-CH_3$ pendant groups of the PDMS; (ii) the well-known strong and immediate chemical bonding between thiol and metal surfaces.[15] The strength of binding between −SH and metal is underscored by the failure of metal transfer when we used methyl-terminated alkanethiol SAMs. The binding strength of the thiol to Au is believed to be the same as that published for Au nanoparticle or cluster surfaces,[30,31] where the bonding occurs through the thiol end and the S−H bond is cleaved upon S−Au chemisorption.

Conclusions

We have exploited the flexibility of PDMS stamps to generate various metal thin-film patterns from stamps with only straight-edge surface features. Roof collapse of the stamp results in new shapes controlled by the stamp dimensions. Au, Ag, and Co metal thin-film patterns with ∼20−40 nm thickness were readily printed onto an alkanedithiol SAM surface with high efficiency. These initial examples have feature size ranging from 50 μm to 2 mm, with edge roughness from 0.25 to 1 μm. Electronic transport measurements for the metal−SAM−metal features are underway. There are several major advantages to this approach: (i) the stamp masters need only have flat edges, for a simpler fabrication process; (ii) the features are uniform over the entire wafer surface, allowing large arrays to be formed in parallel; (iii) the feature size, separation, relief height, stamp elasticity, and external force control the morphology or even appearance of the shapes. These initial examples show that stamp deformation is a new strategy for the microfabrication and potentially nanofabrication of various metal thin-film features and shapes.

Acknowledgment. This work was performed in part at the Cornell Nanofabrication Facility (a member of the National Nanofabrication Users Network) which is supported by the National Science Foundation under Grant ECS-9731293, its users, Cornell University, and Industrial Affiliates.

References and Notes

(1) Shinjo, T.; Okuno, T.; Hassdorf, R.; Shigeto, K.; Ono, T. *Science* **2000**, *289*, 930.

(2) Painter, O.; Lee, R. K.; Scherer, A.; Yariv, A.; O'Brien, J. D.; Dapkus, P. D.; Kim, I. *Science* **1999**, *284*, 1819.

(3) Colombelli, R.; Srinivasan, K.; Troccoli, M.; Painter, O.; Gmachl, C. F.; Tennant, D. M.; Sergent, A. M.; Sivco, D. L.; Cho, A. Y.; Capasso, F. *Science* **2003**, *302*, 1374.

(4) Ohtera, Y.; Ohkubo, H.; Miura, K.; Sato, T.; Kawashima, T.; Kawakami, S. *Opt. Eng.* **2004**, *43*, 1022.

(5) Choi, H. W.; Jeon, C. W.; Dawson, M. D. *J. Cryst. Growth* **2004**, *268*, 527.

(6) Demers, L. M.; Ginger, D. S.; Park, S.-J.; Li, Z.; Chung, S.-W.; Mirkin, C. A. *Science* **2002**, *296*, 1836.

(7) Okazaki, S. *J. Vac. Sci. Technol. B* **1991**, *9*, 2829.

(8) Jeong, H. J.; Markle, D. A.; Owen, G.; Pease, F.; Grenville, A.; von Bünau, R. *Solid State Technol.* **1994**, *37*, 39.

(9) Pease, R. F. W. *J. Vac. Sci Technol. B* **1992**, *10*, 278.

(10) Brambley, D.; Martin, B.; Prewett, P. D. *Adv. Mater Opt. Electron.* **1994**, *4*, 55.

(11) Steingrüber, R.; Golka, S.; Heidrich, H. *Microelectron. Eng.* **2003**, *67*−*68*, 157.

(12) Arshak, K.; Mihov, M. *J. Optoelectron. Adv. Mater.* **2005**, *7*, 193.

(13) Piner, R. D.; Zhu, J.; Xu, F.; Hong, S.; Mirkin, C. A. *Science* **1999**, *283*, 661.

(14) Kumar, A.; Whitesides, G. M. *Appl. Phys. Lett.* **1993**, *63*, 2002.

(15) Xia, Y.; Whitesides, G. M. *Angew. Chem., Int. Ed.* **1998**, *37*, 550.

(16) Tien, J.; Nelson, C. M.; Chen, S. S. *PNAS* **2002**, *99*, 1758.

(17) Tan, L.; Kong, Y. P.; Bao, L.-R.; Huang, X. D.; Guo, L. J.; Pang, S. W.; Yee, A. F. *J. Vac. Sci. Technol. B* **2003**, *21*, 2742.

(18) Rogers, J. A.; Bao, Z.; Baldwin, K.; Dodabalapur, A.; Crone, B.; Raju, V. R.; Kuck, V.; Katz, H.; Amundson, K.; Ewing, J.; Drzaic, P. *Proc. Natl. Acad. Sci. U.S.A.* **2001**, *98*, 4835.

(19) Loo, Y.-L.; Willett, R. L.; Baldwin, K. W.; Rogers, J. A. *Appl. Phys. Lett.* **2002**, *81*, 562.

(20) Loo, Y.-L.; Willett, R. L.; Baldwin, K. W.; Rogers, J. A. *J. Am. Chem. Soc.* **2002**, *124*, 7654.

(21) Loo, Y.-L.; Hsu, J. W. P.; Willett, R. L.; Baldwin, K. W. West, K. W.; Rogers, J. A. *J. Vac. Sci. Technol. B* **2002**, *20*, 2853.

(22) Loo, Y.-L.; Lang, D. V.; Rogers, J. A.; Hsu, J. W. P. *Nano Lett.* **2003**, *7*, 913.

(23) Zaumseil, J.; Meitl, M. A.; Hsu, J. W. P.; Acharya, B. R.; Baldwin K. W.; Loo, Y.-L.; Rogers, J. A. *Nano Lett.* **2003**, *9*, 1223.

(24) Gates, B. S.; Whitesides, G. M. *J. Am. Chem. Soc.* **2003**, *125*, 14986.

(25) Delamarche, E.; Schmid, H.; Michel, B.; Biebuyck, H. *Adv. Mater.* **1997**, *9*, 741.

(26) Sharp, K. G.; Blackman, G. S.; Glassmaker, N. J.; Jagota, A.; Hui. C. *Langmuir* **2004**, *20*, 6430.

(27) Bietsch, A.; Michel, B. *J. Appl. Phys.* **2000**, *88*, 4310.

(28) Hui, C. Y.; Jagota, A.; Lin, Y. Y.; Kramer, E. J. *Langmuir* **2002**, *18*, 1394.

(29) Guo, Q.; Teng, X.; Yang, H. *Nano Lett.* **2004**, *4*, 1657.

(30) Hasan, M.; Bethell, D.; Brust, M. *J. Am. Chem. Soc.* **2002**, *124*, 1132.

(31) Shi, W.; Sahoo, Y.; Swihart, M. T. *Colloids and Surf., A* **2004**, *246*, 109.